The Pontine Nuclei are an Integrative Cortico-Cerebellar Link Critical for Dexterity

Jian-Zhong Guo*, Britton Sauerbrei*, Jeremy D. Cohen, Matteo Mischiati, Austin Graves, Ferruccio Pisanello, Kristin Branson, Adam W. Hantman

*These authors contributed equally.

Summary

Cerebral cortex and cerebellum are thought to interact bidirectionally during movement, motor planning, Pavlovian conditioning, and cognitive function. The pontine nuclei (PN), which consist of the basal pontine nuclei and the reticulotegmental nucleus, constitute the principal hub that convey descending signals from higher brain areas into the cerebellum. The PN receive a massive input from layer 5 of nearly the entire ipsilateral cerebral cortex, and they are thought to serve as a relatively simple relay of this information to both the cerebellar cortex and cerebellar nuclei. Although PN neurons occupy an important anatomical position, little is known about their firing properties during natural movement, feedback effects on cortical activity, or functional role in behavior. Here, we use electrophysiological recordings along with optogenetic and pharmacogenetic perturbations to reveal three key aspects of PN function. First, during the execution of a cortically-dependent reach-to-grab behavior, many PN neurons respond to the movement or to non-motor events, such as the cue signaling trial start. Some neurons respond to both motor and non-motor events, suggesting that the PN do not simply relay separate channels of information into cerebellum, but perform multimodal integration. Second, motor cortical neurons that receive feedback from the ponto-cerebellar system have distinct functional properties during behavior. Third, perturbations of PN function impair performance of reaching, disrupt limb kinematics, and alter the functional responses of motor cortical neurons during movement. Taken together, these results demonstrate that the PN are a rich integrative hub that are essential for dexterous motor control.

Introduction

The integration of ascending signals from the periphery with descending signals from higher brain regions is a widespread motif in the central nervous system. The cerebellum, for instance, receives information from nearly every sensory modality, and ascending pathways carrying vestibular (Barmack, 2003), cutaneous (Bower and Woolston, 1983), proprioceptive (Bosco and Poppele, 2001), and visual (Stone and Lisberger, 1990) stimuli have been studied in detail. These sensory inputs often overlap with inputs from the pontine nuclei (PN) carrying descending information from higher brain areas such as cerebral cortex (Huang et al., 2013). This cerebellar integration of descending motor commands with delayed sensory feedback may enable estimation of the state of the arm, cancellation of the sensory consequences of self-generated movements, and correction for motor errors (Wolpert et al., 1998). Although the descending inputs are widespread and likely critical for cerebellar computation, they are understood more poorly than the ascending pathways.

The pontine nuclei (PN), which include the basal pontine nuclei and reticulotegmental nucleus, are the principal route through which descending signals from cerebral cortex

are conveyed to the cerebellum (Brodal and Jansen, 1946; Brodal and Bjaalie, 1992; Cajal, 1898; Mihailoff et al., 1985). The PN receive massive input from layer 5 of nearly the entire ipsilateral cortex (Leergaard et al., 2004; Legg et al., 1989), as well as descending inputs from the superior colliculus and other structures (Mihailoff et al., 1989). Conversely, ascending pathways such as the medial lemniscus system contribute only a minor input to the PN (Kosinski et al., 1988). The sole output target of the PN is the cerebellum. PN axons mostly terminate in the lateral and intermediate cerebellar cortex (Biswas et al., 2019; Huang et al., 2013), but some also project to the cerebellar nuclei (Mihailoff, 1993). The pontine nuclei have been estimated to be the source of over half of the mossy fiber inputs to the cerebellum.

While the PN are a major hub in the brain (Gao et al., 2018), physiological recordings from the PN during awake behavior have been challenging, due to the difficulty of targeting deep brain structures. Single-unit recordings from the PN in nonhuman primates have revealed responses during arm and eye movements (Matsunami, 1987; Tziridis et al., 2009). During eyeblink conditioning in rabbits, neurons have responses locked to the acoustic tone or resembling the time course of the learned eyeblink, and these eyeblink-related responses are attenuated by cooling of the interpositus nucleus (Clark et al., 1997). In rats, individual neurons have also been found to respond both to acoustic tones and light flashes (Campolattaro et al., 2011), and studies in anesthetized animals have revealed that inputs from different cortical areas may converge onto individual PN neurons (Potter et al., 1978; Ruegg and Wiesendanger, 1975). To date, however, few recordings have been obtained from the PN during the execution of cortically-dependent, voluntary movement.

Although damage to the PN in humans results in motor impairments (Schmahmann et al., 2004), selective PN lesions in animal models have been difficult, as such lesions tend to also damage the corticospinal and medial lemniscus tracts, which run directly through the middle of the nuclei. Nonetheless, the effects of PN lesions have been studied, and the most prominent impairments have involved visual sensorimotor behaviors (Stein and Glickstein, 1992) and gap crossing (Jenkinson and Glickstein, 2000). Similarly, pointing to a moving visual target was also disrupted (Levesque et al., 1986). Recently, hints of the role of the PN in movement execution were found in a joystick task with semi-acute perturbations (Wagner et al., 2019). Therefore, it is still unclear what specific role the PN play in the execution of cortically-dependent voluntary movements.

In order to study the contribution of the PN to skilled behavior, we wanted to use a task requiring brain regions that provide descending input to the PN. We have previously shown that the motor cortex is required for a task in which mice reach and grasp a pellet of food following an acoustic cue; we therefore used this task to interrogate PN function (Guo et al., 2015) (Fig. 1A). We found that the activity of PN neurons was modulated both by movement and by non-motor events, and that disruption of PN function degraded task performance and altered cortical activity patterns.

Results

Firing properties of PN neurons during a dexterous, cortically-dependent behavior.

Although the PN are the major source of descending input to cerebellum, little is known about the activity of PN neurons during behavior. Because the regions of the PN receiving motor cortical input are small and deep in the brain, we targeted our recordings using a combination of high-density electrophysiology and optogenetic stimulation of corticopontine fibers. We performed the experiments in Sim1-Cre X Ai32 mice, which express ChR2 in layer 5 pyramidal tract neurons projecting to the PN. During the recording session, we slowly lowered a 960-site, 384-channel Neuropixels probe (Jun et al., 2017) coated in fluorescent dye towards the PN. As the probe approached its target, we stimulated forelimb motor cortex with an optical fiber coupled to a 473 nm laser using a one-second, 10 Hz pulse train. This resulted in bursts of spiking activity in the target zones, verifying that the probe was in a region of the pontine nuclei receiving motor cortical input (Fig. 1B-C). The cortically-evoked depth profile was later compared with histology to further verify the targeting.

We recorded the activity of 129 PN neurons, which exhibited a wide variety of patterns during the task (Fig. 1D-F). Some cells had firing rate increases or decreases locked to the acoustic cue (e.g. example neuron 1 in Fig. 1D; n = 25), others to the reaching movement (neuron 2; n = 38), and others to both (neuron 3; n = 36). Furthermore, for each of these classes, some neurons were tagged by cortical stimulation (e.g. neurons 2 and 3 in Fig. 1D; n = 30 total tagged neurons), and others were not (fig. 1F). The existence of PN neurons that receive input from motor cortex and respond both to the cue and during movement suggests that the PN are not simply a relay that delivers unprocessed cortical signals to the cerebellum; rather, it is a hub that integrates different modalities of cortical information.

Some neurons exhibited cue-locked firing rate increases that were sustained for several seconds after the cue. In some cases, the offset of these responses coincided with the movement of the hand back to the perch (Supplementary Fig. 1A), but in other cases, they continued for several seconds after the end of the movement (Supplementary Fig. 1B).

In rodents, there appear to be few local inhibitory neurons within the pontine nuclei. Inhibitory inputs to the PN have been identified in the zona incerta, anterior pretectal nucleus, and reticular formation (Border et al., 1986), but it is unclear whether these circuits can be recruited by descending cortical signals to suppress PN spiking. In order to identify possible cortically-driven feedforward inhibition onto PN neurons, we delivered a two-second, 40 Hz sinusoidal laser stimulus to cortex. Some neurons (n = 26) maintained elevated firing rates during this long stimulation, but others showed a sustained decrease (n = 12; Fig. 1G). This suggests that motor cortex is capable not only of exciting PN neurons through direct pyramidal tract projections, but also suppressing them through polysynaptic inhibitory routes.

Motor cortical neurons receiving ponto-cerebellar feedback have distinct functional profiles.

The PN not only receive input from cortex, but also provides feedback through the cerebellum and thalamus. In order to examine ponto-cerebellar feedback to cortex, we induced expression of ChR2 in PN neurons by injecting AAV-FLEX-rev-ChR2-tdTomato into Slc17a7-Cre mice (Huang et al., 2013) and implanting an optical fiber over the PN. We then trained the mice to perform the reach-to-grab task and recorded from

ensembles of motor cortical neurons (n = 749) during the behavior. To identify cortical neurons receiving feedback from the ponto-cerebellar system, we stimulated PN neurons with 473 nm light using a laser coupled to the implanted fiber (10-40 Hz sine wave, 2 s, 8-20mW). PN stimulation evoked transient spiking responses in many neurons (Fig. 2A-B; n = 211). We then examined the firing patterns of PN-tagged and non-PN-tagged cortical neurons during the reaching behavior, by comparing pre- and post-lift spike counts (see Methods). While both tagged and non-tagged neurons exhibited lift-locked increases and decreases, firing rate increases were much more common among tagged neurons (Fig. 2B-C; chi-square test, p = 5e-23). Furthermore, among the cells with firing rate increases, the tagged neurons increased their activity earlier than the non-tagged neurons (Fig. 2D). This suggests that cortical neurons receiving input from the ponto-cerebellar pathway may play a role in movement initiation, rather than being engaged only for feedback corrections of ongoing movements.

Pharmacological inactivation of the PN impairs dexterous reach-to-grab.

We have demonstrated that the PN contain rich signals related to the cortically-dependent reach-to-grab behavior. What impact do these signals have on the execution of this task? In order to address this question, we studied the effect of pharmacologically inactivating the PN outputs. We induced expression of the modified human M4 muscarinic receptor hM4D (Roth, 2016), which reduces neural activity when it binds clozapine-N-oxide (CNO), in the PN. Following this injection, we trained the mice to perform the reach-to-grab behavior, and to perform the task in blocks of three sessions, with systemic injection of saline on the first and third days, and of CNO on the second day (Fig. 3A). Expression of the hM4D receptor in PN neurons receiving motor cortical input was verified after the experiment with histology (Fig. 3B). Following pharmacological inactivation of the PN, the mice were not grossly ataxic, but reached to the pellet with relatively normal hand trajectories (Fig. 3C-D). However, the success rate for the first reach was severely impaired, decreasing from 67% to 45% (Fig. 3E, right, black curve; Supplementary Fig. 2A-B). A similar drop in success rate occurred for subsequent reaches, when the animal attempted to correct for the failed first reach (Fig. 3E, right, gray curve; Supplementary Fig. 2A-B). This decrease in success following CNO injection was not observed in control animals which did not express the hM4D receptor (Fig. 3E, right). Most animals also exhibited an increase in reaction time (Supplementary Fig. 2A-B) and a small increase in hand spread (Supplementary Fig. 2D) following PN inactivation. The decrease in success rate under PN inactivation likely reflects impairment in the fine coordination of the fingers which we were unable to detect by hand tracking, rather than proximal deficits. Thus, PN perturbation does not appear to produce ataxia or impair movement initiation, but rather has a specific effect on the skillful performance of a cortically-dependent reaching behavior.

Optogenetic perturbation of the PN perturbs hand kinematics, impairs reach-to-grab performance, and alters firing patterns of motor cortical neurons during behavior.

Although pharmacogenetic inactivation allowed us to perform a loss-of-function test of the role of the PN, this experiment had several limitations. First, because the effect of the drug is not rapidly reversible, it is possible the animals were able to partially compensate for drug-induced deficits over the course of the session. Second, because

the control and CNO sessions were performed on different days, it was not possible to record the activity of the same motor cortical neurons under the two conditions. Third, it is possible that inactivation is less effective at disrupting movement than an artificial increase in PN activity. In order to address these limitations, we performed rapid, reversible perturbation of the PN with ChR2 stimulation while recording from motor cortex. We interleaved trials with both the start cue and a 2 s, 10-40 Hz sinusoidal laser stimulation with control trials in which only the cue was given (Fig. 4A). In contrast with the pharmacogenetic results, we observed robust kinematic effects of optogenetic perturbation. In many sessions, the animals consistently overreached the target in the forward direction during PN perturbation (Videos 1-2, Fig. 4B). The position of the hand at grab shifted and became more variable on perturbation trials (Fig. 4C-D). Laser stimulation reduced the success rate for the first reach (Fig. 4E, left), and this drop in success tended to occur because the animal overreached the target (Fig. 4E, right). Thus, PN perturbation induces hypermetric reaches and impairs successful grasping; this could reflect either a change in motor commands descending to the spinal cord from the cerebellum, or altered feedback from the cerebellum to motor cortex.

If the perturbation acts in part through feedback to cortex, then lift-aligned motor cortical firing patterns should differ on control and laser trials. Some neurons exhibited a firing rate increase at the onset of the laser, but a similar firing pattern to the control trials during reaching (Fig. 4F, left). Others, however, had different firing patterns during or following the movement (Fig. 4F, right, center). In order to quantify the differences between firing patterns on control and laser trials across the population, we split the neural population according to whether there was an increase in firing rate aligned to the start of the laser, as in Fig. 2. Then, we examined the difference in lift-aligned firing rate Z-scores between laser and control. For PN-tagged neurons, firing rates were elevated before lift on laser trials; this would have been expected based on the phasic laser-onset-aligned responses shown in Fig. 2A. These tagged neurons also exhibited a later response, which began late in the movement and was sustained until over two seconds after lift (Fig. 4G, left). On the other hand, non-PN-tagged neurons did not show a difference, in average, between control and laser trials (Fig. 4G, right). The hypermetric reaches observed on laser trials may have been driven, in part, by the elevated activity of PN-tagged neurons near the end of the reach (Fig. 4G, left).

Discussion

In this study, we have explored the activity patterns in PN neurons during a cortically-dependent reach-to-grasp task. Individual PN neurons receiving motor cortical input could respond not only during the movement, but also to non-motor events. Feedforward inhibition onto PN neurons could be recruited by cortical stimulation. Perturbation of the PN impaired performance, induced hypermetric reaching, and modified movement-locked activity in motor cortex. We also observed that the subset of motor cortical neurons tagged by PN stimulation tended to fire earlier relative to movement onset than those that were not tagged. Taken together, these results establish the PN as a critical hub linking motor cortex and the cerebellum and supporting the execution of skilled movement.

Previous work has suggested that different modalities of information remain segregated in the pons (Schwarz and Thier, 1995), and that multimodal integration occurs within the cerebellar cortex, including at the level of granule cells (Huang et al., 2013). However, we observed many PN neurons that responded both to the cue and to movement onset,

consistent with a previous report of multimodal visual-acoustic responses. Several of these neurons were shown by optogenetic tagging to receive descending input from forelimb motor cortex. This motor cortical input could drive the movement-locked firing rate changes, but the source of cue modulation remains unclear. Thus, the PN are not a simple relay of unimodal descending signals, but integrate signals of multiple modalities. In highly-trained animals performing a self-paced forelimb task, Wagner et al. (2019) observed similar activity patterns in motor cortex and cerebellar granule cells, which might suggest that the PN relay relatively unprocessed signals. The multi-modal integration we observe in the PN might not have been engaged in their task. The logic of multi-modal integration in the PN and how it is engaged in different behaviors remains an important open question.

We have also shown that some PN neurons receive feedforward inhibition driven by forelimb motor cortex. Although inhibitory input to the PN has been demonstrated anatomically (Border et al., 1986), our results show that this inhibition can be recruited by descending cortical input. What is the functional significance of PN inhibition, and when is it engaged? One intriguing possibility is that cortical output is gated off during motor preparation (Kaufman et al., 2014) or the execution of non-cortically-dependent behaviors (Miri et al., 2017).

At the outset of the study, we expected perturbations of the PN to produce a severely ataxic phenotype, similar to those that occur in cerebellar disease . Surprisingly, however, under both pharmacogenetic and optogenetic perturbation, animals were able to produce relatively normal hand trajectories. Optogenetic perturbation of the PN did increase the spread of the hand position at the end point (Fig. 4D), but its most obvious effect was hypermetria: an overreach of the target in the forward direction (Fig. 4B-C). Intriguingly, this kinematic effect was observed only late in the reach, while the early portion of the reach trajectory was normal. Previous work has suggested that optimal feedback control of the arm acts to accurately target the end point of the movement, rather than reflecting the planning of the full trajectory (Todorov and Jordan, 2002). If this were the case, then the late divergence of hand trajectories on control and laser trials could be due to our disruption of a cerebellar state estimate used by motor cortex to control the movement end point.

Perturbation of the PN could influence behavior either through routes that descend from the cerebellum to the spinal cord through the red nucleus and reticular formation, or through feedback effects on motor cortex. Because control and perturbation trials were interleaved in the optogenetics experiments, we were able to compare activity patterns during movement for the same neurons on both trial types. For cortical neurons tagged by PN stimulation, firing rates were elevated late in the movement on laser trials. This suggests that perturbation of the PN changes motor commands in motor cortex, and that such changes may be partially responsible for the hypermetric reaching on laser trials. We cannot exclude the possibility, however, that perturbation-induced changes in cerebellar output that proceed to the spinal cord without feeding back to motor cortex also contribute to the observed hypermetria.

Our study showed that the PN are critical for skillful performance of a dexterous movement. Since the PN receive input from nearly all of cortex, however, they are likely involved in a wide range of non-motor behaviors, as well, and their contribution to more cognitive functions remains a key open question.

Methods

Transgenic mouse lines

Slc17a7-Cre mice were generated by the Janelia Research Campus Gene Targeting and Transgenics Facility, and Pde1c-Cre cryopreserved sperm (line IT106) were obtained from GENSAT (Chip Gerfen; National Institutes of Health, Poolesville, MD) and rederived by the Janelia Research Campus Gene Targeting and Transgenics Facility. Pde1c-Cre (n = 3) and Slc17a7-Cre (n = 5) lines both express Cre recombinase in PN but exhibit different expression patterns elsewhere in the brain. To control for off-target effects, we assessed behavioral phenotypes of both lines. We observed no qualitative behavioral differences between the two mouse lines, and thus used them interchangeably. For the optogenetic perturbations, we used Slc17a7-Cre mice (n = 7). For the electrophysiological recordings in the PN, we obtained mice (n = 6) expressing ChR2 in pyramidal tract neurons by crossing the Cre driver line (Tg(Sim1-Cre)KJ18Gsat, The Jackson Laboratory) to a Cre-dependent ChR2 reporter mouse, Ai32 (Rosa-CAG-LSL-ChR2(H134R)-EYFP-WPRE, The Jackson Laboratory).

Stereotaxic surgeries

Mice (2-5 months old) were anesthetized with 2% isoflurane and placed on a heating pad in a stereotactic frame (Kopf Instruments, Tujunga, CA). A portion of the scalp was removed, the skull was cleaned, and a custom-made headpost was affixed with UV-curing cement (OptiBond, Kerr) or dental acrylic (RelyX Unicem, 3M). For viral injections into the PN, craniotomies were made using a dental drill over the PN (3.90 mm posterior to bregma, 0.4 mm lateral). Injections were bilateral for the pharmacogenetic experiments, and on the left (contra-limb) side for optogenetics experiments. Injection pipettes were made from glass capillaries pulled on a Sutter P-2000 (Novato, CA). Viruses were loaded using a Narishige pneumatic injector (Tokyo, Japan) and injected into the PN at 5.8, 5.6, 5.4, and 5.2 mm below dural surface. Injection volumes were 100 nl each. After each injection, at least two minutes elapsed before proceeding to next depth, and the pipette was withdrawn five minutes after final injection. For the pharmacogenetics experiments, Slc17a7-Cre animals were injected with AAV-2/1-flex-hM4D-GFP or AAV-2/1-flex-hM4D-mCherry. For the ChR2 PN stimulation experiments, Slc17a7-Cre animals were injected with AAV-2/1-CAG-flex-ChR2-TdTomato and implanted with tapered Optogenix fibers in the left PN (Lecce, Italy; NA 0.39, Emission length ~2mm, core diameter 200µm, core+cladding 225µm). For the PN optogenetic perturbation experiments, a craniotomy targeting forelimb motor cortex (bregma +0.5, left 1.7 mm) was sealed with silicone elastomer (Kwik-Sil, WPI). Following surgery, injections of ketoprofen (5 mg/Kg) and buprenorphine (0.1 mg/Kg; Henry Schein Animal Health, Melville, NY) were administered subcutaneously. If animals exhibited signs of pain or distress following surgery, additional doses of either ketoprofen or buprenorphine were administered, as directed by veterinary staff. All procedures were performed in accordance with protocols approved by the Institutional Animal Care and Use Committee (IACUC) of the Janelia Research Campus.

Reach-to-grab task

As described previously, mice undergoing behavioral training were food restricted to 80-90% of original body weight by limiting food intake to 2-3 g/day. Otherwise, mice had ad libitum food. Animals were monitored daily by veterinary staff, according to IACUC guidelines. During training, animals learned to reach for pellets of food with the right paw following a 200 ms, 5 kHz acoustic cue, as described previously. Two high-speed cameras (Point Grey Flea3) with manual iris and focus lenses (Tokina 6-15 mm f/1.4, or

Tamron 13VM1040ASIR 10-40mm, f/1.4) were placed in front and to the right of the animal. A custom-made infrared LED light source was mounted behind each cameras. Video was recorded using BIAS acquisition software (IO Rodeo, available at https://bitbucket.org/iorodeo/bias). The cameras, acoustic cue and table, and laser were controlled using Wavesurfer software (Adam Taylor, Janelia Scientific Computing; http://wavesurfer.janelia.org/) and a custom Arduino controller (Peter Polidoro, Janelia Experimental Technology).

Video analysis

The position of the hand was tracked using the APT software package (https://github.com/kristinbranson/APT), developed by the Branson Lab at Janelia, as described previously. The position of the hand was manually annotated for training frames, a tracker was created using the cascaded pose regression algorithm, and the tracker was applied to all movies in each dataset. The three-dimensional position of the hand was triangulated by performing a stereo calibration of the pair of cameras using the Caltech Camera Calibration Toolbox for Matlab (http://www.vision.caltech.edu/bouguetj/calib_doc/). The timing of behavioral waypoints, including lift and grab, was estimated with the Janelia Automatic Animal Behavior Annotator (https://github.com/kristinbranson/JAABA), as described previously. Lift was defined as initial separation between paw and perch. Hand-open was defined as fingers beginning to separate from palm. Grab was defined as paw moving downwards as digits closed. Supination was defined as wrist rotation >90° upwards. At-mouth was defined as the frame in which the paw was within 1 pixel of mouth. Chew was defined as mastication of pellet visible in mouth. Each behavior classifier inputs a short sequence of frames from both the front- and side-view videos, and outputs a prediction of whether the mouse is performing the given behavior or not in the center frame (note that a different classifier is trained for each behavior and each mouse). The classifier used Histogram of Oriented Gradient (HOG) and Histogram of Optical Flow (HOF) features, general-purpose features that represent the directions and magnitudes of edge and motion vectors. Following the initial classification, post-processing was performed in which the per-frame classification results were smoothed by filling short gaps, and spurious short detection bouts were removed. We further filtered the detected events by considering only event sequences in which a lift, hand-open, and grab were detected in order. Using the JAABA interface, the user manually checked for and corrected classifier errors and retrained the classifier, if necessary. Trials were regarded as “single-grab successes” if the first lift-hand-open-grab sequence resulted in the animal grabbing the pellet, bringing it to the mouth, and chewing. Trials were regarded as “multi-grab successes” if the animal missed on the first attempt, but subsequently grabbed the pellet, brought it to the mouth, and chewed.

Electrophysiological recordings from the PN

On the day prior to recording, a craniotomy was made over the PN (A/P: -3.5-4.0mm, M/L: 0.2-0.5mm, D/V: 5.5-6.0mm) in Sim1-Cre X Ai32 mice (n = 6) and sealed with silicone elastomer (Kwik-Sil, WPI). On the recording day, the animal was head-fixed, a fiber coupled to a 473 nm laser (LuxX 473-80, Omicron Laserage) was placed over forelimb motor cortex, and a 384-channel Neuropixels 3A probe (https://www.neuropixels.org/) coated in a fluorescent dye (CM-DiI, DiI, DiO, Thermofisher Scientific; JF-669, Tocris) was slowly lowered into the brain. As the probe approached the PN, layer 5 motor cortical neurons were activated with a 10 Hz train of 5 ms pulses (2-10 mW), and the depth profile of evoked spiking was examined online. When it was determined that the bottom ~1 mm of the probe was in the PN, the

craniotomy and recording probe were sealed with Kwik-Sil, and after 15 min the reaching task was initiated. Neuropixels data and timestamps for the camera and laser were acquired with a custom FPGA-based system. Electrophysiological data were spike sorted using JRClust (James Jun, https://github.com/JaneliaSciComp/JRCLUST). For offline assessment of the depth profile of evoked spiking, the data for each channel were blanked from 0-6 ms following pulse onset to remove the optical artifact, high-pass filtered with a cutoff of 650 Hz, full-wave rectified, averaged over all pulses, and smoothed over time with a σ = 333 μs Gaussian kernel. Next, the data were spatially smoothed across the probe using a σ = 30 μm Gaussian kernel, and the depth profile averaged between a temporal offset of 6-10 ms from pulse onset was plotted (Fig. 1B, red curve). Units on the bottom 1 mm of the probe were included for analysis; this is the region that the histology and depth profiles suggested to be in the PN. In order to determine whether each neuron responded to the cue, lift, and laser pulse, we counted the spikes occurring immediately before and after each event. The windows used were (-100, 0) and (0, 100) ms for cue and for lift, and (-20, 0) and (0, 20) ms for laser. We then compared the pre- and post-event spike counts using a sign rank test (two-sided for lift and cue, and one-sided for laser), and corrected for multiple comparisons across neurons in each event type using the Benjamini-Hochberg procedure (Fig. 1E-F). Neurons were regarded as modulated by the event if the corrected p-value $q < .05$. Firing rates were visualized by smoothing the cue-aligned spike trains using a σ = 50 ms Gaussian kernel, Z-scoring based on the mean and standard deviation of the firing rate from cue - 1000 ms to cue - 200 ms, and averaging across trials (Fig. 1E.) For the long laser stimuli (Fig. 1G), spike counts were again compared between the 2 s laser-on period and the 2 s pre-laser period using a two-sided sign rank test. Firing rates were classified as changing during the laser if $q < .05$.

Pharmacogenetic manipulations

Selective expression of the hM4D DREADD receptor was induced in the PN by injecting AAV-2/1-flex-hM4D-GFP or AAV-2/1-flex-hM4D-mCherry into the PN of Slc17a7-Cre (n = 5) or Pde1c-Cre (n = 3) mice, as described above. Following this injection, mice were trained to perform the reach-to-grab task until they achieved success rates of ~50-80%. Then, they were subjected to multiple three-day testing sequences (Fig. 3A). On the first day ("pre-CNO"), they were given a systemic injection of 0.9% saline immediately before being head-fixed and performing the task. On the second day, CNO (6 μg/g) was administered before the task, and on the third day, saline was given again. This three-day sequence was repeated several times for each mouse once behavior had stabilized. The same procedure was applied to control mice (n = 4) that did not express the hM4D receptor.

Optogenetic perturbations and electrophysiological recordings from motor cortex

Selective expression of ChR2 was induced in the PN by injecting Slc17a7-Cre mice (n = 7) with AAV-2/1-CAG-flex-ChR2-TdTomato in the left PN and implanting a tapered optical fiber over the injection site, as described above. Animals were trained on the reach-to-grab task, and a craniotomy over forelimb motor cortex (bregma +0.5 mm, left 1.7 mm) was performed before the first day of recording. During the recording session, an optical coupler attached to a 473 nm laser (LuxX 473-80, Omicron Laserage) was attached to the connection on the top of the skull leading to the tapered fiber. A four-shank, 64-channel probe (Janelia Experimental Technology) was lowered to approximately 900 μm below the surface of forelimb motor cortex. The 16 recording sites on each shank had a range of 0 to 320 μm from the tip of the shank. During the experiment, three types of trials were administered: (1) control trials, in which a cue was

given and the table rotated to provide the food pellet, (2) laser-only trials, in which a 2 s, 10Hz or 40Hz sinusoidal laser stimulus was given with no cue, and (3) laser-cue trials, in which the laser was given either synchronously with the cue, or 200 ms before the cue. The laser power at the tip of the coupler was measured at 8-20 mW, but there was likely a significant power drop between the coupler and the fiber in the brain. Lift-aligned hand trajectories in the forward direction were compared by visualizing the control and laser trajectories (Fig. 4B, right), and by computing the two-sided t-statistic for control and laser position at each time lag (Fig. 4B, left). The position of the hand at the time of grab was extracted for control and laser plots and compared by plotting (Fig. 4C), and by computing the spread, defined to be the sum of the standard deviations for each of the three spatial dimensions, for control and laser trials (Fig. 4D, left). Success rates for Fig. 4D-E refer to success on the first grab attempt. In order to assess whether cortical neurons were modulated during movement and by PN stimulation, we compared paired spike counts for each trial immediately before and after lift or laser onset using a sign-rank test (two-sided for lift, one-sided for laser). The pre- and post-lift windows were (-1000, -500) and (-50, 450), and the pre- and post-laser windows were (-150, 0) and (0, 150) ms. A Benjamini-Hochberg correction for multiple comparisons was applied, and neurons were classified as modulated by the lift or laser if the corrected p-value $q < .05$ (Fig. 2D). For assessing the laser-aligned responses, we included both laser-only trials and laser-cue trials in which no lift occured in the post-laser window; using laser-only trials alone did not qualitatively change the results. Lift-aligned firing rates were visualized by smoothing the spike trains with a $\sigma = 50$ ms Gaussian kernel, Z-scoring based on the mean and standard deviation of the firing rate within a window of (-1000, -400) ms of lift, and averaging across trials (Fig. 2B, 4G.)

Author contributions and acknowledgements

J.G. performed behavioral experiments and cortical recordings and analyzed behavior data. B.S. analyzed electrophysiology and behavior data and generated the figures. J.C. performed Neuropixels recordings in the PN. M.M. analyzed electrophysiology and behavior data. A.G. performed preliminary slice experiments and analyzed behavior data. F.P. developed and fabricated the optical fibers for PN stimulation. K.B. developed video analysis tools and analyzed behavior data. B.S., M.M., and A.H. wrote the paper with input from all authors. A.H. supervised the project. We thank Gülşen Sürmeli, Diana Burk, and Cheng-Chu Huang for help with pilot experiments, Adam Taylor for Wavesurfer software, Tim Harris and the Neuropixels Consortium for probe development, James Jun for spike sorting software, and Steve Edgley, Amy Bastian, Stephen Scott, Daniel Wolpert, and Brett Mensh for discussions.

Figure captions

Figure 1: Firing properties of PN neurons during a cortically-dependent reach-to-grab task. (A) Behavioral task and reach kinematics. Upper: mice were head-fixed and trained to reach to and grasp a pellet of food following an acoustic cue. Lower: example hand trajectories aligned to the cue. The green dots indicate lift, when the animal initiates the reach-to-grab sequence. (B) Strategy for recording from motor-cortex-recipient neurons in the pontine nuclei. An optical fiber was placed over the forelimb motor cortex of mice expressing ChR2 in pyramidal tract neurons (Sim1-Cre X Ai32). A 384-channel Neuropixels probe was lowered into the pontine nuclei as a laser pulse train was delivered to cortex. The depth profile of evoked multi-unit activity (red trace) revealed a zone of corticorecipient sites at the bottom of the probe. The grayscale histological section shows the location of the bottom of the probe in the pontine nuclei. (C) Raw data

from six channels near the bottom of the probe showing activity evoked by motor cortex stimulation. (D) Spike rasters and firing rates for example neurons in the task. The timing of lift is indicated by the green dots. The panels on the right show each unit's response to cortical stimulation. (E) Firing rate Z-scores for each neuron, sorted according to whether the cell responded to the cue, the lift, or both. Cyan ticks indicate which neurons were tagged by stimulation of motor cortex. (F) Venn diagram indicating the number of neurons responding to different combinations of the cue, lift, and cortical stimulation. (G) Response of PN neurons to a two-second stimulation of motor cortex. Upper: firing rate Z-scores for each neuron, aligned to laser onset. Blue ticks indicate neurons with a sustained increase, and red ticks indicate neurons with a decrease. Lower: laser-aligned spike rasters and firing rate for an example neuron suppressed by motor cortical stimulation.

Figure 2: Motor cortical neurons receiving feedback from the ponto-cerebellar system have distinct functional properties during reaching. (A) Identification of cortical neurons tagged by PN stimulation. Upper: experimental schematic. Animals expressing ChR2 in the PN were implanted with an optical fiber for optogenetic stimulation. A silicon probe was inserted into forelimb motor cortex to record neural activity during the task. At the beginning of the session, PN neurons were stimulated with 473 nm light. Lower: raw data example showing cortical spiking locked to the onset of PN stimulation. Each trace is a single trial. (B) Movement-locked neural activity for PN-tagged (n = 228) and non-PN-tagged (n = 521) cortical neurons; n = 32 sessions, n = 7 mice, and n = 749 total recorded neurons. Left: firing rate heatmaps aligned to movement onset (lift) for PN-tagged neurons. Many neurons had increased activity around lift, and a few had decreased activity. Right: firing rate heatmaps for non-PN-tagged neurons. Approximately equal numbers of neurons had firing rate increases and decreases around lift. (C) Table showing the percentages of tagged and non-tagged neurons with increases, decreases, or no change in activity around lift. (D) PN-tagged neurons have distinct properties during movement. Upper: average firing rate Z-scores for tagged and non-tagged neurons with firing rate increases around lift. The average activity for the tagged group increased earlier than the activity for the non-tagged group. Lower: distribution of the timing of firing rate peaks for tagged and non-tagged neurons. PN-tagged neurons had earlier firing rate peaks than non-tagged neurons.

Figure 3: Pharmacogenetic inactivation of the pontine nuclei disrupts prehension success rate. (A) Experimental design. (B) Histology of hM4D expression from a trained Pde1c-Cre mouse. Image of PN neurons expressing hM4D, labeled in red, and forelimb motor cortical axons, labeled in green. Magnified view of boxed region shows residence of hM4D-expressing neurons in forelimb M1 terminal field. (C) Hand trajectories during the pre-CNO, CNO, and post-CNO sessions for the mouse in (B). Insets show close-ups of hand position at grab. (D) Forward, right, and upward hand trajectories for all sessions of each type from the same mouse. (E) Left: success rates for single-grab and multi-grab reaches (when the animal attempted again after an initial failure) for all mice expressing the hM4D receptor (n = 8 mice; n = 90 sessions). Right: success rates for control mice without the hM4D receptor (n = 4 mice; n = 24 sessions). Error bars are 95% confidence intervals.

Figure 4: Optogenetic perturbation of the PN alters motor cortical activity and induces hypermetric reaches. (A) Experimental schematic. Mice expressing ChR2 in the PN were implanted with a fiber to allow stimulation of PN neurons while population activity was recorded in motor cortex. On control trials, the cue was delivered, and the mouse

reached to the target. On laser trials, a 2 s PN stimulation was delivered, aligned to the cue. Data are from the same sessions as for Fig. 2. (B) Hypermetric reaching under PN stimulation. Left, t-statistic indicating difference between the forward position of the hand in laser and control trials. Each row corresponds to one session. Blue indicates that the hand was farther forward on laser trials; yellow indicates that it was farther back. Right, average hand trajectories in the forward direction on control and laser trials for three example datasets. Error bars indicate standard error of the mean. (C) Three-dimensional position of the hand at the time of grab on control and laser trials for each of the three example datasets in (B). Each point corresponds to a single trial. (D) Left: spread of the hand (sum of the standard deviations in each direction) on control and laser trials. Each point is one session. Blue points indicate a difference in success rate on the first grab ($q < .05$, chi-square test). Right: difference in spread between laser and control versus the distance between mean hand position at grab for laser and control. (E) Left, success on first grab attempt for laser versus control trials. Right, difference in forward hand position (lift +100 to +300 ms) between laser and control versus success rate difference between laser and control. (F) Spike rasters and firing rates on laser and control trials for three example neurons. Black dots indicate the start of laser stimulation. (G) Left, difference in peri-lift firing rate z-scores between control and laser trials for neurons tagged by PN stimulation. Error bars show standard error of the mean across neurons, and the shaded gray region corresponds to the window of lift -100 to +300 ms shown in Fig. 4B. Right, difference in firing rate z-scores for non-tagged neurons.

Supplementary figure 1: Long-duration responses in PN neurons. (A) A PN neuron that exhibits a cue-locked response and maintains an elevated firing rate while the hand is in an upward position. The grayscale heatmap indicates upward hand position, magenta ticks are spike times, and green dots are lift times. (B) Another example neuron, as in (A). This neuron maintains an elevated firing rate for the entire four-second window.

Supplementary figure 2: Characterization of behavioral effects of pharmacogenetic inactivation of the PN. (A) Table showing success rates, reaction times, and lift-to-grab duration for each mouse. (B) Scatterplots of the data in (A) for the CNO vs pre-CNO sessions. (C) Three-dimensional hand position at grab for each mouse in the CNO (red) and pre-CNO (gray) sessions. (D) Left, spread in hand position at grab (sum of standard deviations for each spatial dimension) for CNO vs pre-CNO sessions. Right, change in spread between CNO and pre-CNO sessions versus shift in mean position.

Video 1: Behavior on a control (cue-only) trial for an animal with ChR2 and an optical fiber in the PN.

Video 2: Behavior on a laser + cue trial for the animal from video 1. The animal keeps overreaching the target as long as the laser is on.

References

Barmack, N.H. (2003). Central vestibular system: vestibular nuclei and posterior cerebellum. Brain Res Bull *60*, 511-541.

Biswas, M.S., Luo, Y., Sarpong, G.A., and Sugihara, I. (2019). Divergent projections of single pontocerebellar axons to multiple cerebellar lobules in the mouse. J Comp Neurol.

Border, B.G., Kosinski, R.J., Azizi, S.A., and Mihailoff, G.A. (1986). Certain basilar pontine afferent systems are GABA-ergic: combined HRP and immunocytochemical studies in the rat. Brain Res Bull *17*, 169-179.

Bosco, G., and Poppele, R.E. (2001). Proprioception from a spinocerebellar perspective. Physiol Rev *81*, 539-568.

Bower, J.M., and Woolston, D.C. (1983). Congruence of spatial organization of tactile projections to granule cell and Purkinje cell layers of cerebellar hemispheres of the albino rat: vertical organization of cerebellar cortex. J Neurophysiol *49*, 745-766.

Brodal, A., and Jansen, J. (1946). The ponto-cerebellar projection in the rabbit and cat; experimental investigations. J Comp Neurol *84*, 31-118.

Brodal, P., and Bjaalie, J.G. (1992). Organization of the pontine nuclei. Neurosci Res *13*, 83-118.

Cajal, S.R. (1898). Histology of the Nervous System.

Campolattaro, M.M., Kashef, A., Lee, I., and Freeman, J.H. (2011). Neuronal correlates of cross-modal transfer in the cerebellum and pontine nuclei. J Neurosci *31*, 4051-4062.

Clark, R.E., Gohl, E.B., and Lavond, D.G. (1997). The learning-related activity that develops in the pontine nuclei during classical eye-blink conditioning is dependent on the interpositus nucleus. Learn Mem *3*, 532-544.

Gao, Z., Davis, C., Thomas, A.M., Economo, M.N., Abrego, A.M., Svoboda, K., De Zeeuw, C.I., and Li, N. (2018). A cortico-cerebellar loop for motor planning. Nature *563*, 113-116.

Guo, J.Z., Graves, A.R., Guo, W.W., Zheng, J., Lee, A., Rodriguez-Gonzalez, J., Li, N., Macklin, J.J., Phillips, J.W., Mensh, B.D*., et al.* (2015). Cortex commands the performance of skilled movement. Elife *4*, e10774.

Huang, C.C., Sugino, K., Shima, Y., Guo, C., Bai, S., Mensh, B.D., Nelson, S.B., and Hantman, A.W. (2013). Convergence of pontine and proprioceptive streams onto multimodal cerebellar granule cells. Elife *2*, e00400.

Jenkinson, E.W., and Glickstein, M. (2000). Whiskers, barrels, and cortical efferent pathways in gap crossing by rats. J Neurophysiol *84*, 1781-1789.

Jun, J.J., Steinmetz, N.A., Siegle, J.H., Denman, D.J., Bauza, M., Barbarits, B., Lee, A.K., Anastassiou, C.A., Andrei, A., Aydin, C.*, et al.* (2017). Fully integrated silicon probes for high-density recording of neural activity. Nature *551*, 232-236.

Kaufman, M.T., Churchland, M.M., Ryu, S.I., and Shenoy, K.V. (2014). Cortical activity in the null space: permitting preparation without movement. Nat Neurosci *17*, 440-448.

Kosinski, R.J., Lee, H.S., and Mihailoff, G.A. (1988). A double retrograde fluorescent tracing analysis of dorsal column nuclear projections to the basilar pontine nuclei, thalamus, and superior colliculus in the rat. Neurosci Lett *85*, 40-46.

Leergaard, T.B., Alloway, K.D., Pham, T.A., Bolstad, I., Hoffer, Z.S., Pettersen, C., and Bjaalie, J.G. (2004). Three-dimensional topography of corticopontine projections from rat sensorimotor cortex: comparisons with corticostriatal projections reveal diverse integrative organization. J Comp Neurol *478*, 306-322.

Legg, C.R., Mercier, B., and Glickstein, M. (1989). Corticopontine projection in the rat: the distribution of labelled cortical cells after large injections of horseradish peroxidase in the pontine nuclei. J Comp Neurol *286*, 427-441.

Levesque, F., Fabre-Thorpe, M., Wiesendanger, M., and Buser, P. (1986). Brachium pontis lesions in cats partly reproduce the cerebellar dysfunction of voluntary reaching movements. Behav Brain Res *21*, 167-181.

Matsunami, K. (1987). Neuronal activity in nuclei pontis and reticularis tegmenti pontis related to forelimb movements of the monkey. Neurosci Res *5*, 140-156.

Mihailoff, G.A. (1993). Cerebellar nuclear projections from the basilar pontine nuclei and nucleus reticularis tegmenti pontis as demonstrated with PHA-L tracing in the rat. J Comp Neurol *330*, 130-146.

Mihailoff, G.A., Kosinski, R.J., Azizi, S.A., and Border, B.G. (1989). Survey of noncortical afferent projections to the basilar pontine nuclei: a retrograde tracing study in the rat. J Comp Neurol *282*, 617-643.

Mihailoff, G.A., Lee, H., Watt, C.B., and Yates, R. (1985). Projections to the basilar pontine nuclei from face sensory and motor regions of the cerebral cortex in the rat. J Comp Neurol *237*, 251-263.

Miri, A., Warriner, C.L., Seely, J.S., Elsayed, G.F., Cunningham, J.P., Churchland, M.M., and Jessell, T.M. (2017). Behaviorally Selective Engagement of Short-Latency Effector Pathways by Motor Cortex. Neuron *95*, 683-696 e611.

Potter, R.F., Ruegg, D.G., and Wiesendanger, M. (1978). Responses of neurones of the pontine nuclei to stimulation of the sensorimotor, visual and auditory cortex of rats. Brain Res Bull *3*, 15-19.

Roth, B.L. (2016). DREADDs for Neuroscientists. Neuron *89*, 683-694.

Ruegg, D., and Wiesendanger, M. (1975). Corticofugal effects from sensorimotor area I and somatosensory area II on neurones of the pontine nuclei in the cat. J Physiol *247*, 745-757.

Schmahmann, J.D., Ko, R., and MacMore, J. (2004). The human basis pontis: motor syndromes and topographic organization. Brain *127*, 1269-1291.

Schwarz, C., and Thier, P. (1995). Modular organization of the pontine nuclei: dendritic fields of identified pontine projection neurons in the rat respect the borders of cortical afferent fields. J Neurosci *15*, 3475-3489.

Stein, J.F., and Glickstein, M. (1992). Role of the cerebellum in visual guidance of movement. Physiol Rev *72*, 967-1017.

Stone, L.S., and Lisberger, S.G. (1990). Visual responses of Purkinje cells in the cerebellar flocculus during smooth-pursuit eye movements in monkeys. I. Simple spikes. J Neurophysiol *63*, 1241-1261.

Todorov, E., and Jordan, M.I. (2002). Optimal feedback control as a theory of motor coordination. Nat Neurosci *5*, 1226-1235.

Tziridis, K., Dicke, P.W., and Thier, P. (2009). The role of the monkey dorsal pontine nuclei in goal-directed eye and hand movements. J Neurosci *29*, 6154-6166.

Wagner, M.J., Kim, T.H., Kadmon, J., Nguyen, N.D., Ganguli, S., Schnitzer, M.J., and Luo, L. (2019). Shared Cortex-Cerebellum Dynamics in the Execution and Learning of a Motor Task. Cell *177*, 669-682 e624.

Wolpert, D.M., Miall, R.C., and Kawato, M. (1998). Internal models in the cerebellum. Trends Cogn Sci *2*, 338-347.

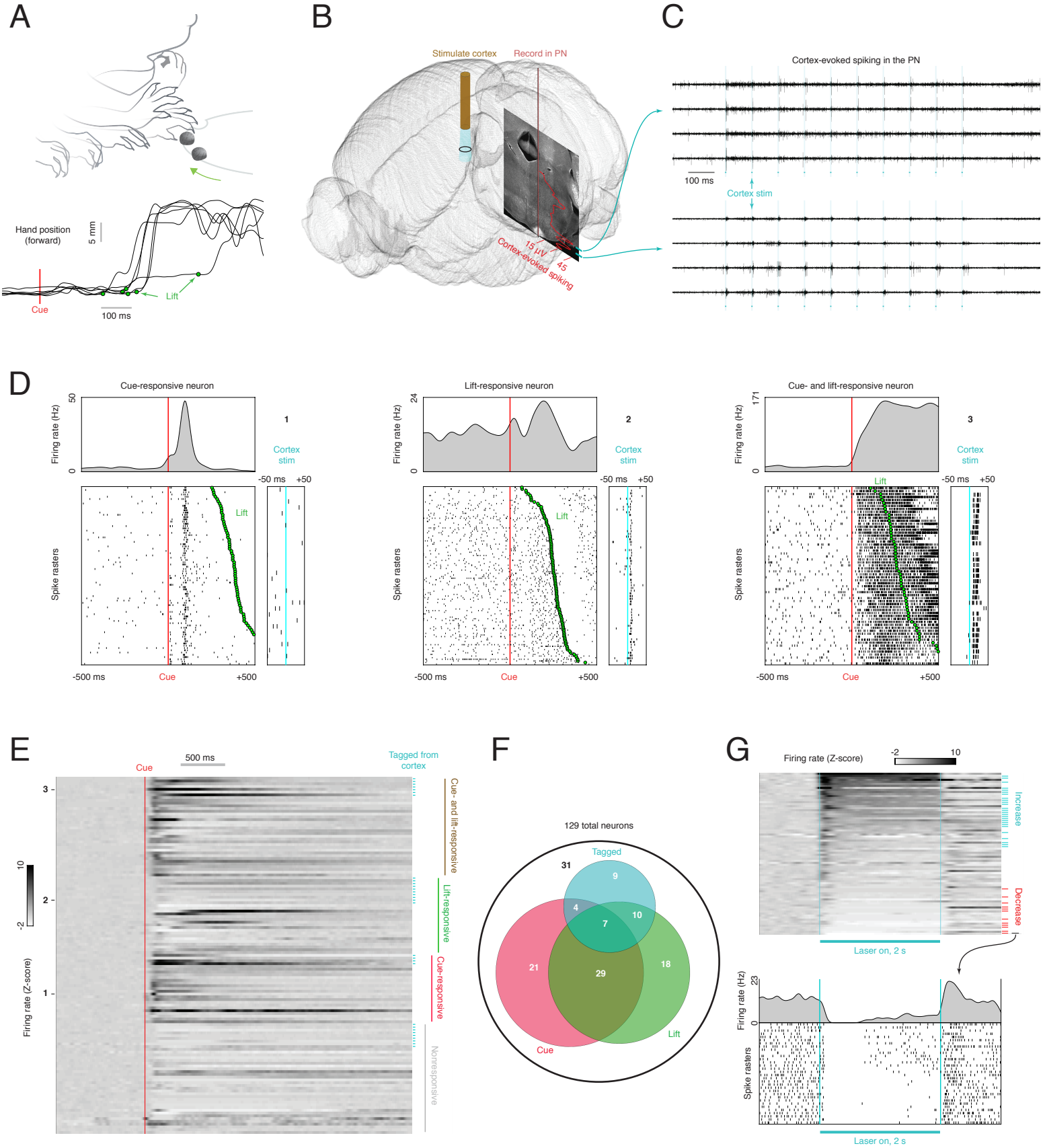
A
Hand position (forward)
5 mm
Cue
Lift
100 ms
B
Stimulate cortex
Record in PN
15 µV
45
Cortex-evoked spiking
C
Cortex-evoked spiking in the PN
100 ms
Cortex stim
D
Cue-responsive neuron
Lift-responsive neuron
Cue- and lift-responsive neuron
Firing rate (Hz)
Spike rasters
Cortex stim
Lift
-50 ms
+50
-500 ms
Cue
+500
E
500 ms
Cue
Tagged from cortex
Firing rate (Z-score)
Cue- and lift-responsive
Lift-responsive
Cue-responsive
Nonresponsive
F
129 total neurons
Tagged
Cue
Lift
31
9
4
10
7
21
29
18
G
Firing rate (Z-score)
Increase
Decrease
Laser on, 2 s
Firing rate (Hz)
Spike rasters

Figure 1

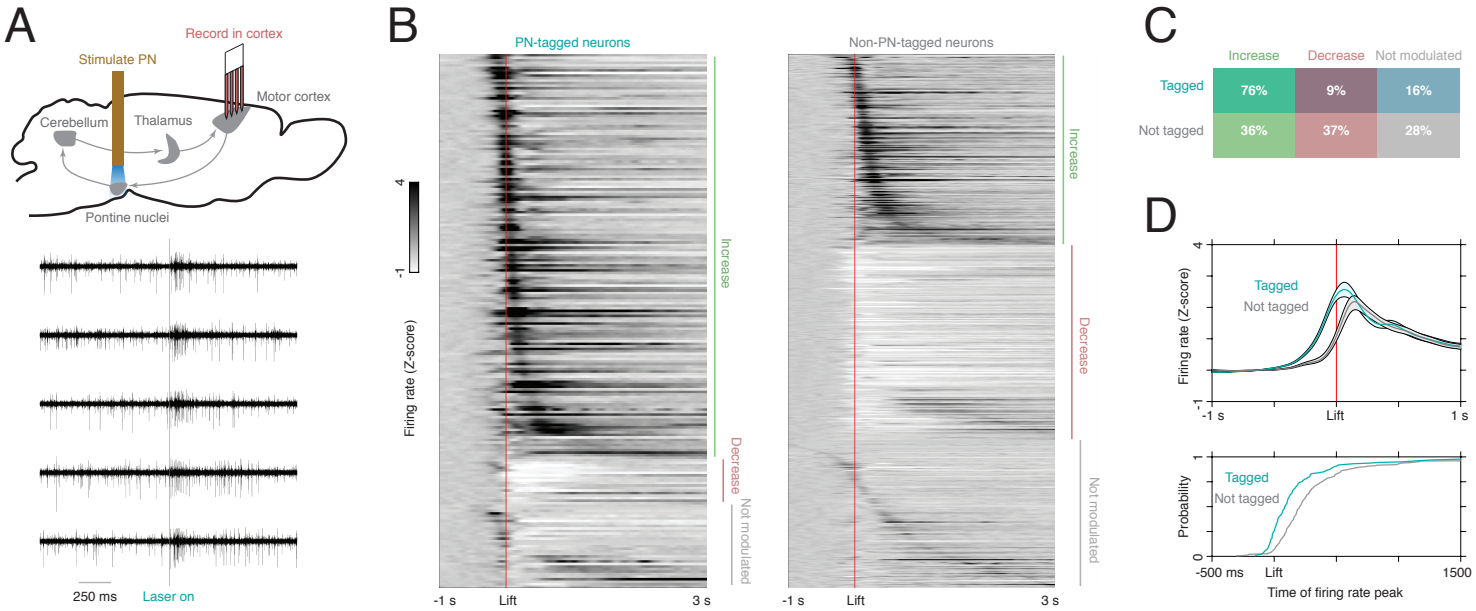
A
Record in cortex
Stimulate PN
Motor cortex
Cerebellum
Thalamus
Pontine nuclei
250 ms
Laser on
B
PN-tagged neurons
Non-PN-tagged neurons
Firing rate (Z-score)
4
-1
Increase
Decrease
Not modulated
-1 s
Lift
3 s
C
Increase
Decrease
Not modulated
Tagged
Not tagged
76%
9%
16%
36%
37%
28%
D
Tagged
Not tagged
Firing rate (Z-score)
-1 s
Lift
1 s
Probability
-500 ms
1500
Time of firing rate peak

Figure 2

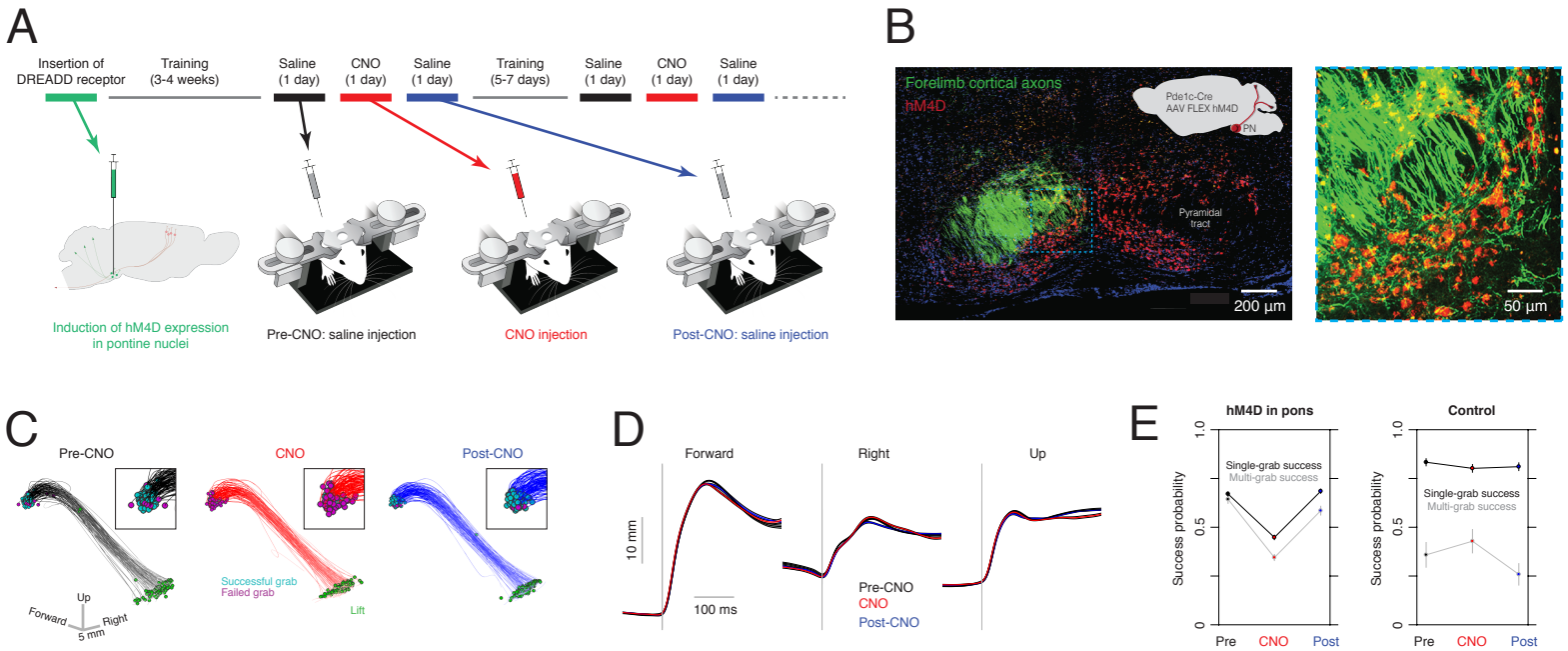
A
Insertion of DREADD receptor
Training (3-4 weeks)
Saline (1 day)
CNO (1 day)
Saline (1 day)
Training (5-7 days)
Saline (1 day)
CNO (1 day)
Saline (1 day)
Induction of hM4D expression in pontine nuclei
Pre-CNO: saline injection
CNO injection
Post-CNO: saline injection
B
Forelimb cortical axons
hM4D
Pde1c-Cre AAV FLEX hM4D
PN
Pyramidal tract
200 µm
50 µm
C
Pre-CNO
CNO
Post-CNO
Successful grab
Failed grab
Lift
Up
Forward
Right
5 mm
D
Forward
Right
Up
10 mm
100 ms
Pre-CNO
CNO
Post-CNO
E
hM4D in pons
Control
Success probability
Single-grab success
Multi-grab success
Pre
CNO
Post

Figure 3

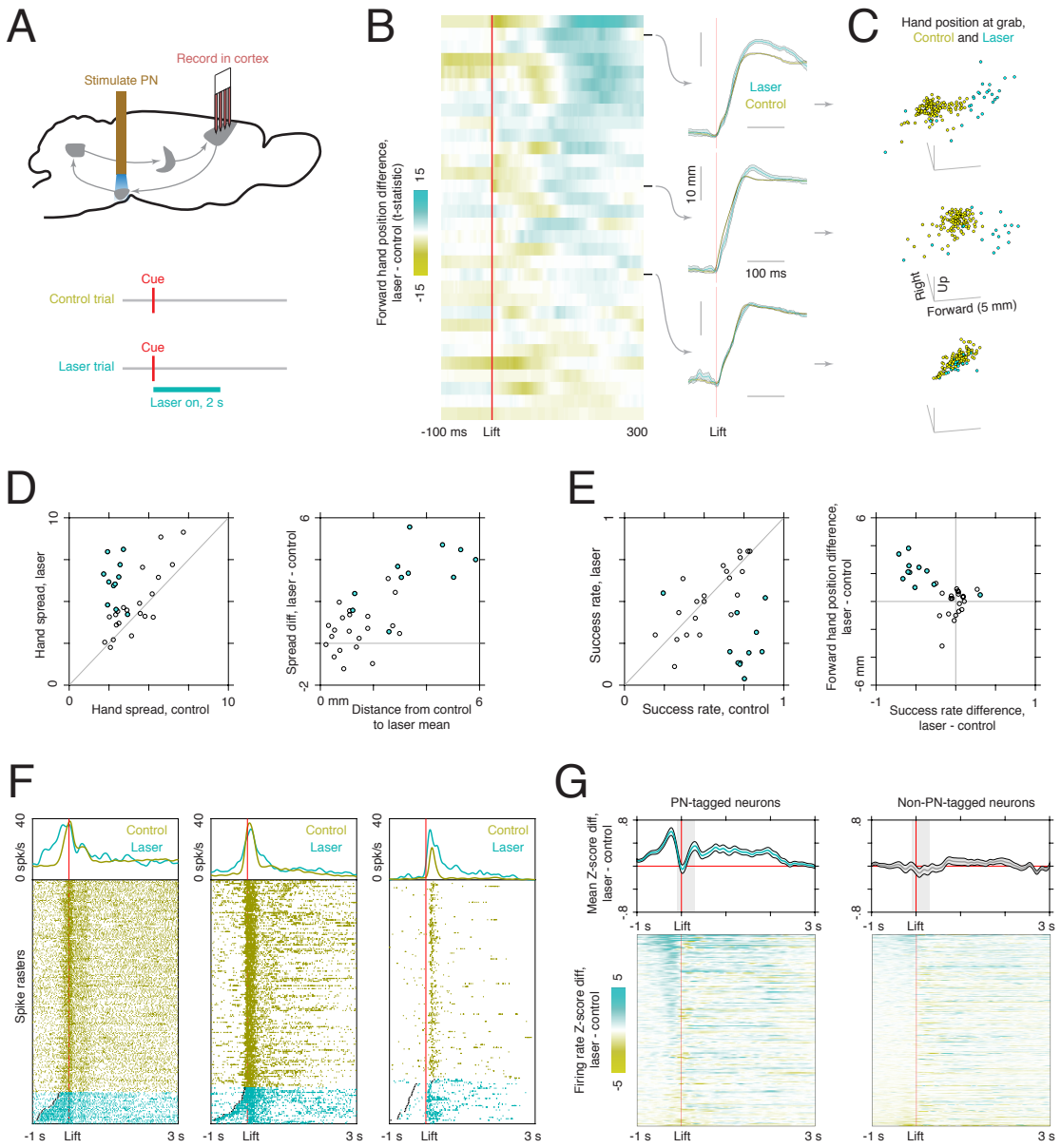
A
Record in cortex
Stimulate PN
Control trial
Cue
Laser trial
Cue
Laser on, 2 s
B
Forward hand position difference, laser - control (t-statistic)
15
-15
-100 ms
Lift
300
Lift
Laser
Control
10 mm
100 ms
C
Hand position at grab, Control and Laser
Right
Up
Forward (5 mm)
D
Hand spread, laser
Hand spread, control
Spread diff, laser - control
0 mm
Distance from control to laser mean
E
Success rate, laser
Success rate, control
Forward hand position difference, laser - control
-6 mm
Success rate difference, laser - control
F
Control
Laser
0 spk/s
40
Spike rasters
-1 s
Lift
3 s
G
PN-tagged neurons
Non-PN-tagged neurons
Mean Z-score diff, laser - control
Firing rate Z-score diff, laser - control
5
-5

Figure 4

A

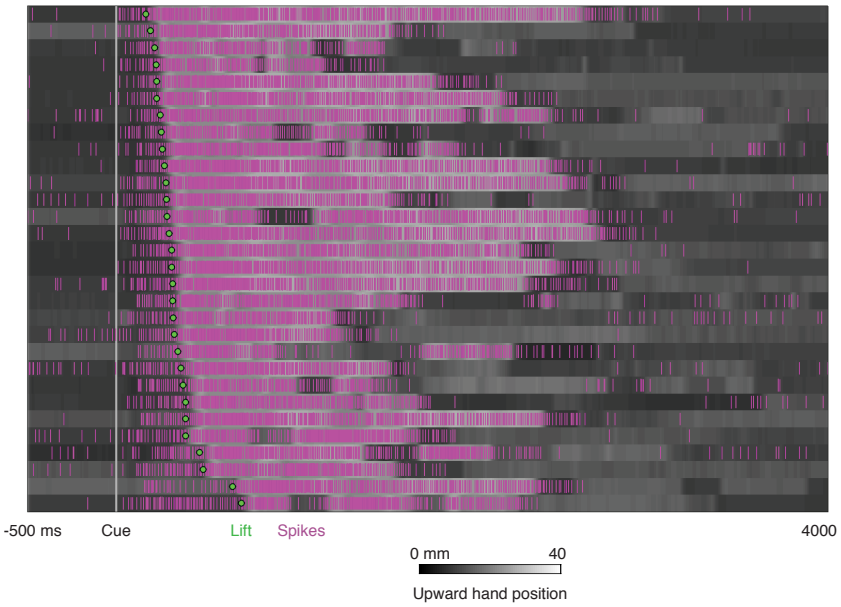

B

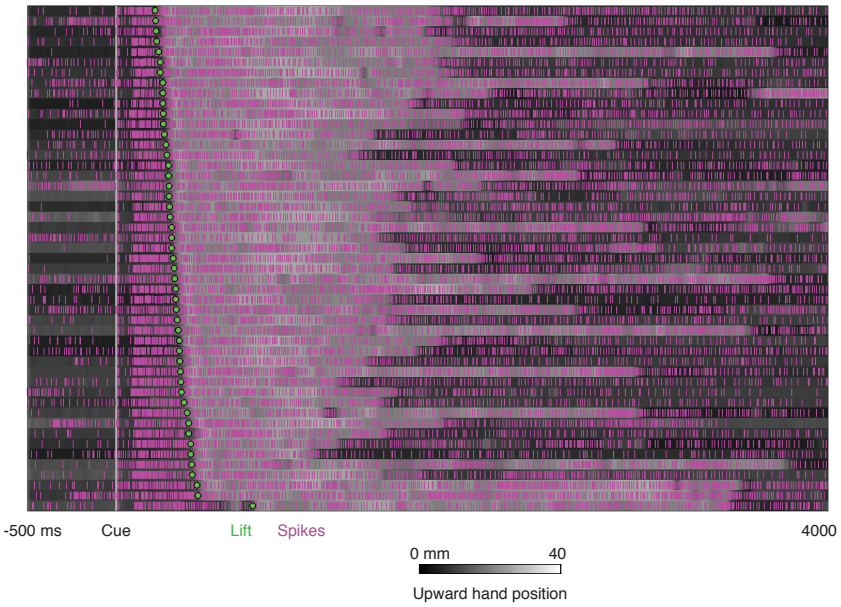

Supplemental Figure 1

A

		Single success rate			Multi success rate			Reaction time (ms)			Lift-to-grab time (ms)		
		Pre-CNO	CNO	Post-CNO	Pre-CNO	CNO	Post-CNO	Pre-CNO	CNO	Post-CNO	Pre-CNO	CNO	Post-CNO
M118	Pde1c-Cre	57%	41%	45%	70%	45%	68%	520	513	426	94	92	107
M119	Pde1c-Cre	77%	23%	79%	57%	11%	62%	297	330	276	121	164	116
M122	Pde1c-Cre	86%	39%	77%	36%	10%	27%	284	282	268	118	112	112
M127	Slc17a7-Cre	69%	49%	63%	64%	28%	54%	247	300	268	95	109	102
M130	Slc17a7-Cre	60%	37%	64%	59%	44%	55%	200	244	222	82	84	84
M186	Slc17a7-Cre	71%	50%	76%	70%	49%	61%	250	288	256	116	114	114
M187	Slc17a7-Cre	46%	44%	55%	68%	33%	56%	266	292	266	94	88	96
M201	Slc17a7-Cre	82%	57%	77%	57%	39%	56%	192	210	200	94	94	92

B

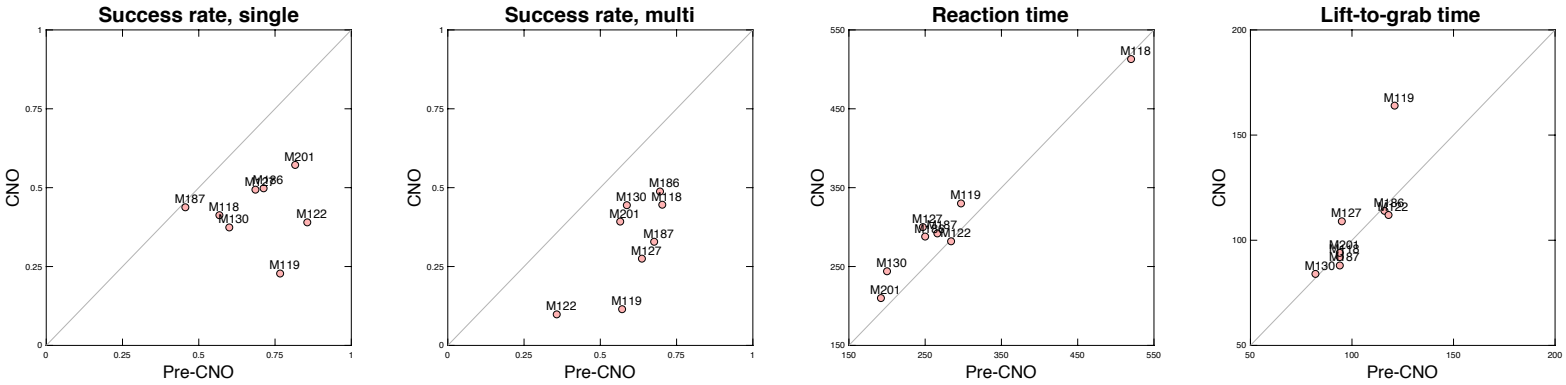

C

D

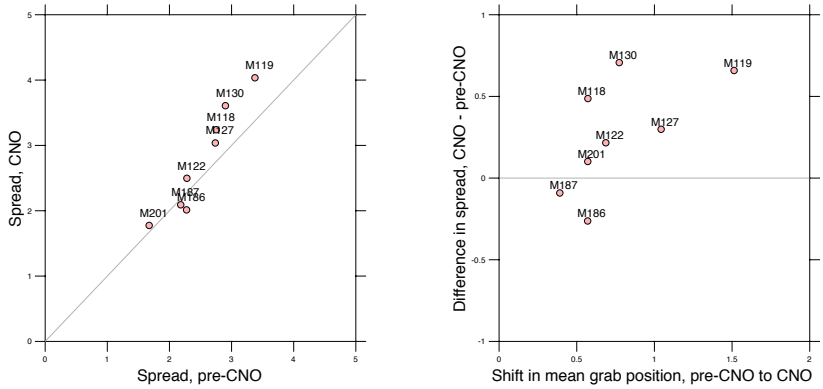

Supplemental Figure 2